Kinetic Monte Carlo Simulations of Low-Temperature NH<inf>3</inf>-SCR over Cu-Exchanged Chabazite

ChemPhysChem

Research Article
doi.org/10.1002/cphc.202400558

Chemistry Europe
European Chemical Societies Publishing

www.chemphyschem.org

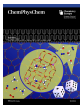

Kinetic Monte Carlo Simulations of Low-Temperature NH_3-SCR over Cu-Exchanged Chabazite

Yingxin Feng*[a] and Henrik Grönbeck*[a]

Cu-exchanged chabazite (Cu-CHA) is widely used for ammonia assisted selective catalytic reduction of nitrogen oxides (NH_3-SCR). The Cu^+ ions are at low temperatures solvated by NH_3 forming mobile $[Cu(NH_3)_2]^+$ complexes. The dynamic behaviour of the complexes is critical as O_2 adsorption requires a pair of complexes to form a $[Cu_2(NH_3)_4O_2]^{2+}$ peroxo-species over which NO couples with NH_3. Here we introduce a first principles-based kinetic Monte Carlo approach to explore the effect of the Al-distribution on the reaction kinetics of NH_3-SCR over Cu-CHA. The method allows us to scrutinize the interplay between the pairing of $[Cu(NH_3)_2]^+$ complexes and the reaction landscape for the NH_3-SCR reaction over the peroxo-complex. The Al-distribution affects the stability of the $[Cu(NH_3)_2]^+$ pairs as well as the kinetic parameters of the SCR-reaction. The turn-over frequency is determined by the stability of the $[Cu(NH_3)_2]^+$ pairs and the relative strength of NO and NH_3 adsorption once a pair is present. The results establish the hierarchy of effects that influences the performance of Cu-CHA over NH_3-SCR and provide a computational basis for further development of the Cu-CHA material.

Introduction

Selective catalytic reduction of nitrogen oxides with ammonia (NH_3-SCR) is used to control nitrogen oxide (NO_x) emissions from exhaust streams with oxygen excess.[1] Copper-exchanged chabazite materials (Cu-CHA) is commercialized for NH_3-SCR thanks to high activity and selectivity over a wide temperature range together with superior hydrothermal stability.[1–3] In exhaust streams with only NO, the overall reaction follows the so-called "standard-SCR reaction":

$$4NH_3 + 4NO + O_2 \rightarrow 4N_2 + 6H_2O \quad \text{(R1)}$$

The stoichiometry includes an equal amount of NO and NH_3. O_2 is required to accommodate the H atoms. O_2 is not needed in exhaust streams with NO_2 where the reaction can proceed according to the "fast-SCR" or "NO_2-SCR" reaction schemes:

$$2NH_3 + NO + NO_2 \rightarrow 2N_2 + 3H_2O \quad \text{(R2)}$$

$$8NH_3 + 6NO_2 \rightarrow 7N_2 + 12H_2O \quad \text{(R3)}$$

Depending on the reaction conditions and Cu-loading, the presence of NO_2 has been measured to enhance or reduce the activity of Cu-CHA.[4,5]

The NH_3-SCR reaction requires a material with redox capacity and the Cu-ions in Cu-CHA alternate between Cu^+ and Cu^{2+}. Activation of O_2 proceeds over Cu^+ forming Cu^{2+}, whereas the coupling between NO and NH_3 reduces Cu^{2+} to Cu^+. The NH_3-SCR activity over Cu-CHA shows a non-monotonic temperature dependence with a minimum at intermediate temperatures. The minimum in activity signals that different reaction mechanisms apply at low- and high-temperatures.[6] At low-temperatures, X-ray absorption spectroscopy (XAS) and density functional theory (DFT) calculations have shown that Cu^+ is solvated by NH_3, forming mobile $[Cu(NH_3)_2]^+$ complexes.[7–12] The measured low-temperature activity has a quadratic dependence on the Cu-loading, which indicates that two $[Cu(NH_3)_2]^+$ complexes are required for O_2 activation.[9,13] Thus, the dynamic behaviour and pairing of the $[Cu(NH_3)_2]^+$ complexes are crucial for the performance. The Cu-complexes diffuse in the zeolite framework and O_2 has a probability to adsorb when two $[Cu(NH_3)_2]^+$ complexes occupy the same CHA cage, forming a $[Cu_2(NH_3)_4O_2]^{2+}$ peroxo-complex.[10,14] Density functional theory calculations have been used to elucidate the NH_3-NO coupling over the peroxo-complex.[15,16] The reaction is strictly sequential where NH_3 reacts with NO adsorbed on the Cu^{2+} site forming H_2NNO. Repeating the reaction yields $[Cu_2(NH_3)_4(OH)_2]^{2+}$, where two NO react with the OH-groups forming two HONO intermediates. H_2NNO and HONO diffuse in the zeolite structure and decompose into N_2 and H_2O over Brønsted acid sites.[15,16] N_2O formation is an unwanted side-reaction, which could occur if H_2NNO decomposes over $[Cu_2(NH_3)_4OOH]^{2+}$ instead of a Brønsted acid site.[16,17]

The proposed reaction scheme for low-temperature NH_3-SCR over Cu-CHA has been favorably evaluated using first-principles-based mean-field microkinetic modeling.[6,16,18] The kinetic modeling revealed a competitive NO and NH_3 adsorp-

[a] Y. Feng, H. Grönbeck
Department of Physics and Competence Centre for Catalysis,
Chalmers University of Technology, SE-412 96 Göteborg, Sweden
E-mail: yingxin@chalmers.se
ghj@chalmers.se

Supporting information for this article is available on the WWW under https://doi.org/10.1002/cphc.202400558

tion on the peroxo-complex. The inhibiting effect of NH_3 is in agreement with experiments showing a negative reaction order in NH_3. Having a detailed mean-field model, it has been shown that the reaction kinetics can be described accurately by a simplified model with only five reaction steps: adsorption of O_2, NH_3 and NO together with lumped reactions for N_2 and N_2O formation.[18] The simplified model can describe the reaction as O_2 adsorption is the first step in the sequential reaction and NO adsorption has rate control due to the inhibiting effect of NH_3.[16]

The previous first principles-based microkinetic models[6,16,18] are based on the mean-field approach, which assumes a homogeneous lattice of active sites and a random distribution of adsorbates. Moreover, the models have not targeted the pairing of $[Cu(NH_3)_2]^+$ complexes but instead assumed the existence of a complex pair allowing for O_2 adsorption. To account for the probability of having a $[Cu(NH_3)_2]^+$ pair, the turnover frequency was scaled in Refs. [16,18] with a Boltzmann factor accounting for the energy difference between separated and paired complexes. For a certain Al-distribution,[9] this factor has been estimated to be about 6×10^{-4}, thus, significantly affecting the absolute turnover frequency. Although the mean-field approach reproduces measured reaction orders in O_2, NO and NH_3, as well as the apparent activation energy, it does not capture the effects of sample heterogeneity. Importantly, density functional theory calculations predict that the Al-distribution influence the stability of the $[Cu(NH_3)_2]^+$ pairs,[19] which affects the probability of O_2 adsorption and the subsequent NO-NH_3 coupling. To understand how the Al-distribution influences the reaction kinetics, it is needed to go beyond mean-field approaches.

Here, we introduce a DFT-based kinetic Monte Carlo (kMC) method to study NH_3-SCR over Cu-CHA. The approach allows us to explicitly treat the diffusion of $[Cu(NH_3)_2]^+$ complexes within the CHA framework and reveal how the Al-distribution influences the reaction kinetics via the interplay between $[Cu(NH_3)_2]^+$ pairing and NO-NH_3 coupling. Kinetic Monte Carlo simulations[20,21] have been used in the past to explore structure-dependent kinetics, arising from heterogeneous surfaces and nanoparticles.[22–24] For the NH_3-SCR reaction over Cu-CHA, we find that the stability of $[Cu(NH_3)_2]^+$ pairs largely determines the absolute turn-over frequency. However, the relative strength of NO and NH_3 adsorption onto $[Cu_2(NH_3)_4O_2]^{2+}$ affects significantly the activity once a Cu-complex pair is formed. The kinetic parameters for CHA-cages with different properties are based on DFT calculations for the stability of Cu-complex pairs as well as NO and NH_3 adsorption. The kMC approach to the NH_3-SCR reaction allows us to link specific Al-distributions to a high probability of complex pairing and efficient NO-NH_3 coupling, which can be used to develop catalysts with enhanced performance.

Computational Methods

First-Principles Calculations

The Vienna *ab-initio* Simulation Package (VASP)[25–28] is applied to perform spin-polarized density functional theory calculations. The valence electrons are described using a plane wave basis set with a cutoff energy of 480 eV, and the interaction between the valence and the core electrons is described by the projector augmented wave (PAW) method.[29,30] The number of valence electrons treated in the calculations are Cu(11), Si(4), Al(3), O(6), N(5), and H(1). The k-point sampling is restricted to the gamma point.

The gradient-corrected Perdew–Burke–Ernzerhof (PBE)[31] functional is used to describe exchange-correlation effects. A Hubbard-U term of 6 eV is added to the Cu 3*d* states to properly describe the Cu–O bond in the $[Cu_2(NH_3)_4O_2]^{2+}$ peroxo complex.[32,33] In addition, a Grimme-D3 correction is applied to account for the van der Waals interactions of the floating molecules and complexes in the zeolite.[34,35] The convergence criterion in the self-consistent field loop is set to be 1×10^{-5} eV, and the structures are considered to be relaxed when the force acting on each atom is less than 0.02 eV/Å.

The periodic chabazite structure is described in the hexagonal unit cell, which contains 36 tetrahedral Si-sites. The experimentally determined lattice parameters ($\alpha = \beta = 90.0^\circ$, $\gamma = 120.0^\circ$; $a = b = 13.803$, $c = 15.075$ Å are used and fixed during the structural optimizations. The Cu-CHA material is modeled by replacing three Si atoms with Al, yielding a silicon-to-aluminum (Si/Al) ratio of 11. The Si/Al ratio is similar to common experimental values.[8,16,36,37] Eight different Al-distributions were selected to study the stability of NH_4^+ formed by NH_3 adsorption on the Brønsted acid sites, separated and paired $[Cu_2(NH_3)_4]^{2+}$ complexes, as well as the NO and NH_3 adsorption onto the peroxo $[Cu_2(NH_3)_4O_2]^{2+}$ complex.

Kinetic Monte Carlo Simulations

Kinetic Monte Carlo (kMC) is a stochastic method where random numbers are used to solve the chemical master equation. The chemical master equation expresses the time evolution of the probability P_α for a system to be in a certain state α:

$$\frac{dP_\alpha}{dt} = \sum_\beta [k_{\alpha\beta}P_\beta - k_{\beta\alpha}P_\alpha] \quad (1)$$

The sum includes all states β that are connected to α via a reaction. $k_{\alpha\beta}$ is the rate constant associated with an event that changes the state of the system. The kMC simulations are performed with the Python program MonteCoffee,[23] which implements the first reaction method.[20] The First-reaction method is based on having a list with possible events. The events are executed in chronological order and the list of times of occurrence for the events is updated after each Monte Carlo step. For each event, the time of occurrence is determined using the corresponding rate constant ($k_{\alpha\beta}$) and a random number:

$$t_{\alpha\beta} = t - \frac{1}{k_{\alpha\beta}} \ln u \quad (2)$$

where t is the current simulation time, which is set to 0 in the beginning of the simulation, and u is a uniform random number on the unit interval. Once an event is executed, t is updated and the list of events is updated by adding events that have been enabled

and removing events that have been disabled. The simulations continue until t has reached a predefined end-time.

The rate constant ($k_{\alpha\beta}$) connecting two states is given by:[38]

$$k_{\alpha\beta} = \frac{k_B T}{h} e^{-\Delta G^{\ddagger}/k_B T} = \frac{k_B T}{h} e^{\Delta S^{\ddagger}/k_B} e^{-\Delta H^{\ddagger}/k_B T} \approx \frac{k_B T}{h} e^{\Delta S^{\ddagger}/k_B} e^{-\Delta E^{\ddagger}/k_B T}$$

Where k_B is Boltzmann's constant, T is the temperature, and h is Planck's constant. The $\Delta G^{\ddagger}$ is the difference in Gibbs free energy between the initial and transition states. $\Delta S^{\ddagger}$ and $\Delta H^{\ddagger}$ are the corresponding differences in entropy and enthalpy, respectively. Because the volume and pressure do not change in the reaction, the change in enthalpy ($\Delta H^{\ddagger}$) can be replaced with the change in energy ($\Delta E^{\ddagger}$). The entropy and energy differences are taken from our previous studies in Refs. [16,18] except for the entropy barrier associated with $[Cu(NH_3)_2]^+$ diffusion between CHA-cages via an 8-membered ring. The entropy of the $[Cu(NH_3)_2]^+$ complex is restricted in the diffusion as the molecular axis should not deviate substantially from the surface normal of the plane defining the 8-membered ring. Allowing for a 10-degree deviation from the surface normal, the entropy of $[Cu(NH_3)_2]^+$ in the transition state is approximated as a one-dimensional translator scaling the rotational entropy accordingly.

Results and Discussions

Our previous mean-field kinetic analysis shows that O_2 adsorption on a pair of $[Cu(NH_3)_2]^+$ complexes, NO adsorption on $[Cu_2(NH_3)_4O_2]^{2+}$ and NH_3 desorption from $[Cu_2(NH_3)_5O_2]^{2+}$ control the reaction.[16] Knowing the rate controlling steps, it has been shown that a simplified model with the rate controlling steps and lumped reactions for N_2 and N_2O formation accurately reproduce the reaction kinetics.[18] Here, the NH_3-SCR reaction is simulated with kMC, which enables an explicit treatment of $[Cu(NH_3)_2]^+$ diffusion and pairing. The reaction steps are based on our simplified model and the considered reaction path is shown in Figure 1. The first step is the pairing of two complexes. Having a pair, the reaction proceeds by O_2 adsorption forming the $[Cu_2(NH_3)_4O_2]^{2+}$ peroxo-complex. The next step is NO adsorption, which competes with NH_3 adsorption.[16] Adsorbed NO reacts with NH_3 from the gas-phase to form N_2 and H_2O. The barriers associated with N_2 and H_2O formation from adsorbed NO do not have rate control[16] and are treated as one lumped reaction step.

Effect of Al-Distribution on Kinetic Parameters

To establish the effect of the Al-distribution on the crucial kinetic parameters, we investigate by DFT calculations the stability of $[Cu(NH_3)_2]^+$ pairs together with NO and NH_3 adsorption for eight different Al-distributions. Here, three Si atoms are replaced by Al and the charge is balanced by adding Cu complexes or NH_4^+. The results are shown in Figure 2 and the different configurations are ordered according to the area of the triangle formed by the three Al atoms. The numbering of the Al atoms is shown in Figure 1. The energies in (a)–(c) are reported with respect to the lowest energy configuration. (d) is the energy difference between paired and separated $[Cu(NH_3)_2]^+$ complexes. (e) is the difference in the adsorption energy of NH_3 and NO.

The stability of the systems with three NH_4^+(a) and two $[Cu(NH_3)_2]^+$ with one NH_4^+ (b,c) is reduced when the Al-ions are close. This is rationalized by the repulsive Coulomb interaction between these cationic species, which is not completely balanced by the interactions with the anionic zeolite sites. The highest stability is obtained for an intermediate area, which provides a balance between the attractive and repulsive

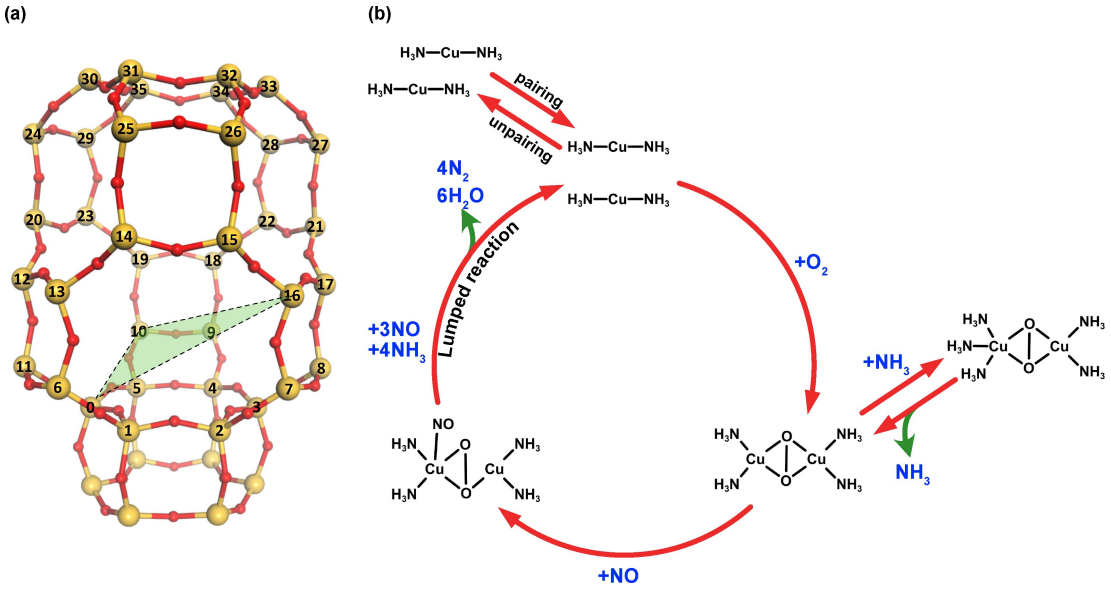

Figure 1. (a) Structural model of the CHA zeolite. The Si-ions are numbered to indicate the placement of Al-ions. Atomic color codes: Si (yellow), and O (red). The green triangular plane illustrates the area of the triangle formed when the three Si are replaced by Al. (b) Considered reaction cycle for low-temperature NH_3-SCR.

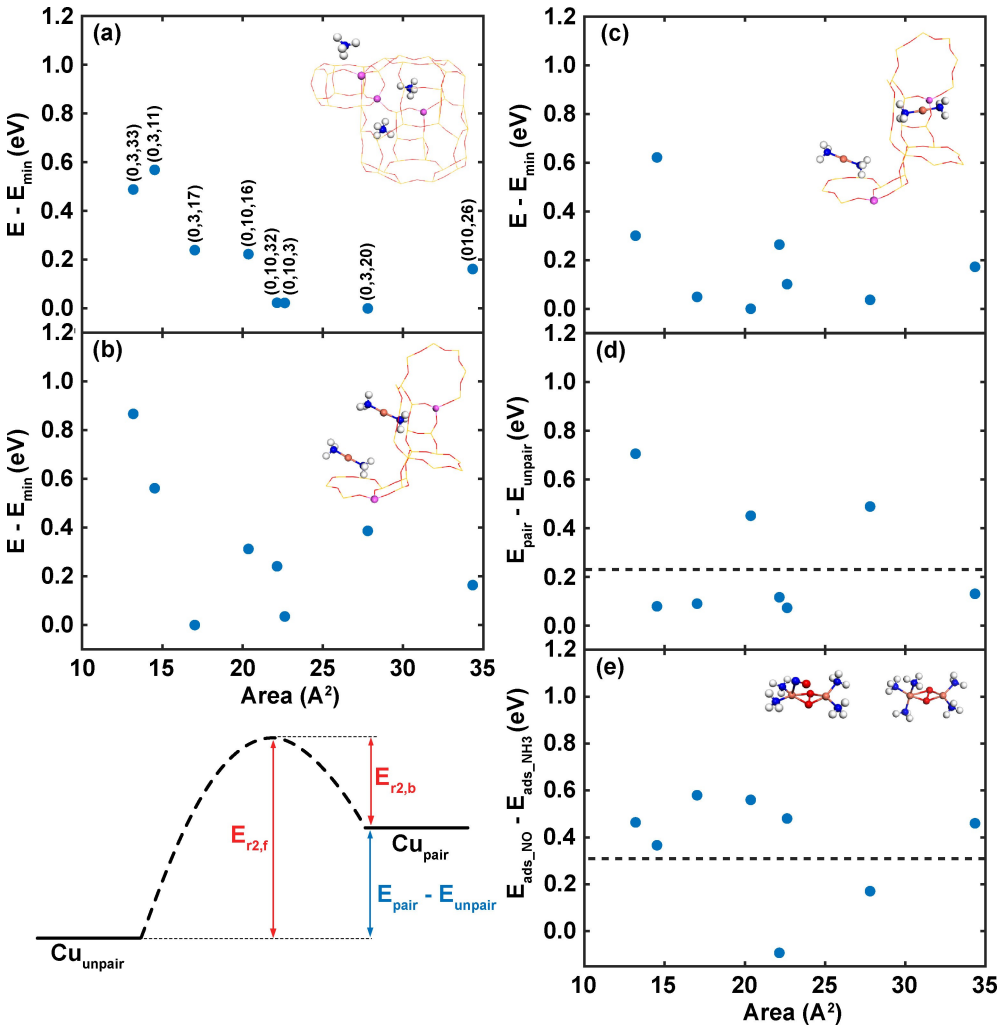

Figure 2. Energy differences for crucial species in CHA with different Al-distribution. (a) Three NH_4^+ ions. (b) Paired $[Cu(NH_3)_2]^+$ complexes. (c) Unpaired $[Cu(NH_3)_2]^+$ complexes. (d) Difference in stability between paired and unpaired complexes. (e) Difference in adsorption energy of NO and NH_3 on $[Cu_2(NH_3)_4O_2]^{2+}$. The configurations are labeled according to the numbering in Figure 1. The dashed lines are the energy difference between paired and unpaired $[Cu(NH_3)_2]^+$ complexes and the energy difference between NO and NH_3 adsorption on the $[Cu_2(NH_3)_4O_2]^{2+}$, respectively used in our previous kinetic model.[16] Atomic color code: Cu (bronze), Si (yellow), Al (pink), O (red), N (blue), and H (white).

Coulomb interactions. The pronounced dependence on the Al-distribution agrees with a previous report.[19]

The difference between having separated and paired complexes (d) shows that unfavorable configurations to some extent can compensated, making the difference within 0.1 eV for five of the studied configurations. However, it is important to note that some pair-configurations are clearly less stable than other configurations. In previous DFT calculation,[9] the difference has been reported to be 0.23 eV, which is shown by a dashed line in Figure 2(d). Our calculations stress that the stability of the $[Cu(NH_3)_2]^+$ pairs varies with the Al-distribution and, thus, affect the stability of $[Cu(NH_3)_2]^+$ pairs. Unstable pairs will have a high probability for separation, see Figure 2. Moreover, unstable pairs will reduce the SCR-activity as pairs are needed to adsorb O_2 forming the $[Cu_2(NH_3)_4O_2]^{2+}$ complex, which is a critical intermediate in the reaction. In the following Monte Carlo simulations, the energy difference between paired and unpaired complexes is denoted ΔE_1.

Having a pair of complexes, the SCR reaction is limited by the competitive adsorption of NO and NH_3. The difference in adsorption energy of NH_3 and NO (denoted ΔE_2) for the different configurations is reported in Figure 2(e). In our previous work, the NH_3 and NO adsorption energies were calculated to be 0.98 and 0.70 eV, respectively.[16] The difference in the adsorption energies (0.28 eV) is shown by a dashed line in Figure 2(e). The difference in the adsorption energies for the different Al-distribution shows a spread and the preference for NH_3 is in most cases larger than in our previous calculation. However, one of the configurations (0, 10, 32) has similar adsorption energies for the two adsorbates.

Kinetic Monte Carlo Simulations

The considered geometry and reaction events are sketched in Figure 3. Each large CHA cage is in the periodic zeolite materials

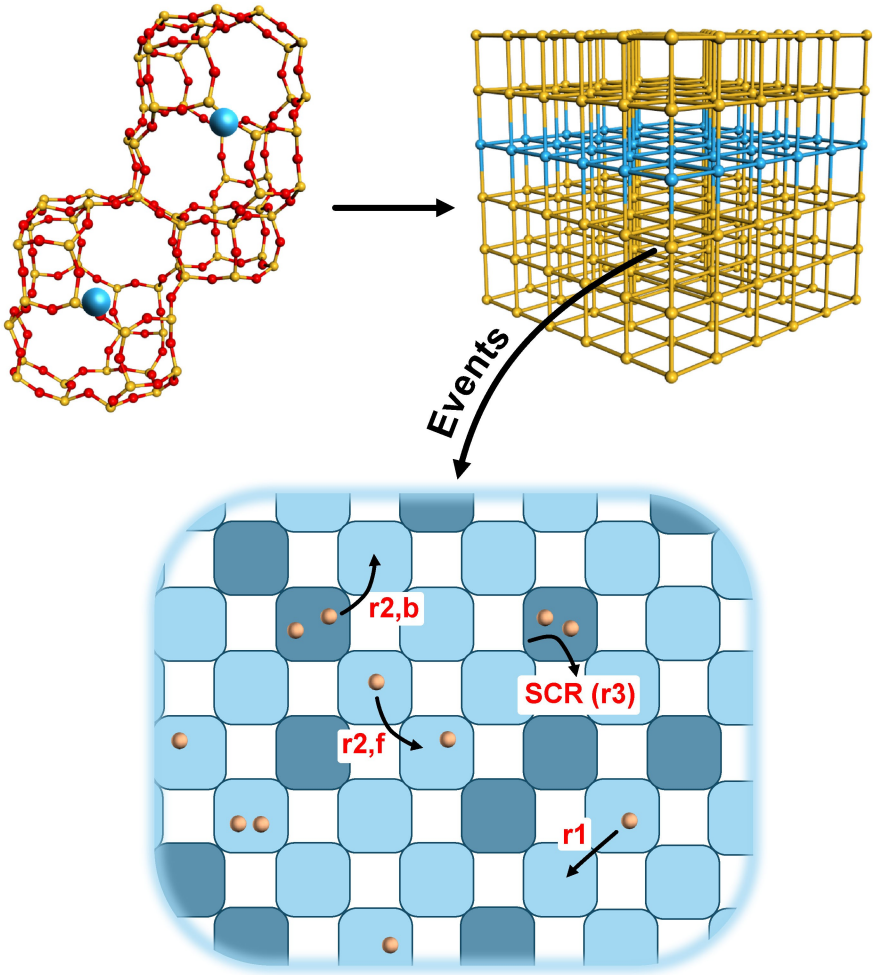

Figure 3. Top: Atomistic model and the cubic lattice representation of the CHA zeolite. The blue marks in the CHA cages constitute the simple cubic lattice. Bottom: The possible events over the lattice model. The different colors in the lattice model represent zeolite cages with different properties.

connected to six neighboring large cages. This connectivity is in the simulations represented by a simple cubic lattice where each node represents a zeolite cage. The material is modeled with a $6 \times 6 \times 6$ lattice applying periodic boundary conditions. The considered events are sketched in a plane of the lattice where the different colors of the lattice points indicate different properties of the CHA-cages modeling the effects of an inhomogeneous Al-distribution.

The reaction follows the simplified reaction cycle in Figure 1 (see also Supporting Information). The events treated explicitly are shown in Table 1. The diffusion of the $[Cu(NH_3)_2]^+$ complex from one cage to another is described by reaction r1. The barrier for diffusion has been calculated to be about 0.3 eV,[9,39] which means that the rate is fast at typical reaction conditions. In kMC simulations, fast events are generally scaled to obtain a sufficient number of reaction events.[40] Here we have used a diffusion barrier of 0.85 eV for diffusion between empty cages. We have verified that the diffusion barrier can be as high as 1.3 eV without affecting the reaction kinetics, see Supporting Information (SI). The possibility to scale the diffusion of the complex without disturbing the kinetics, demonstrates that diffusion of copper complexes is not rate controlling.

Reaction $r2_f$ is the paring event where a $[Cu(NH_3)_2]^+$ complex diffuses to a cage already containing one $[Cu(NH_3)_2]^+$

Table 1. Energy ($\Delta E^{\ddagger}$) and entropy ($\Delta S^{\ddagger}$) contributions to the reaction barriers of the considered steps. Energy is given in eV and entropy in J/mol·K. The $*_a$, $*_b$ represent the connected CHA cages. Cu represents Cu species in the form of $[Cu(NH_3)_2]^+$. $E_{r2,b}$ is the barrier for unparing, which is treated as a parameter in the simulations.

no.	considered step	$\Delta E^{\ddagger}_f$	$\Delta E^{\ddagger}_b$	$\Delta S^{\ddagger}_f$	$\Delta S^{\ddagger}_d$
r1	$Cu^*_a + *_b \xleftrightarrow{r1} *_a + Cu^*_b$	0.85	0.85	26.9	26.9
r2	$Cu^*_a + Cu^*_b \xleftrightarrow{r2} 2Cu^*_a + *_b$	0.85	$E_{r2,b}$	26.9	26.9
r3	$2Cu^*_a + O_2 + 4NO + 4NH_3 \xleftrightarrow{r3} 4N_2 + 6H_2O + 2Cu^*_a$	0.34	14.1	–	–

complex. The separation of a complex pair (unpairing) is described by reaction r2$_b$. The barrier for the unpairing depends on the stability of the pair and, thus, the Al-distribution. Each cage can at most contain two $[Cu(NH_3)_2]^+$ complexes. Reaction r3 is the NH_3-SCR reaction, which is possible over paired complexes. The SCR reaction is treated in a lumped manner and the equilibrium constants are used to describe the probability of having O_2, NH_3, and NO adsorbed on the pair of complexes. Reaction r3 is strongly exothermic, which means that the probability for the backward reaction can be neglected. The O_2, NO and NH_3 adsorption/desorption events are frequent and, therefore, not treated explicitly. Instead, the probability of having O_2 adsorbed on a pair of complexes is given by:

$$P_{O_2} = \frac{K_{O_2}}{1 + K_{O_2}} \tag{4}$$

where K_{O_2} is the equilibrium constant. Using the fact that the reaction is strictly sequential,[16] the probability of having NO adsorbed on the peroxo complex is given by:

$$P_{NO} = \frac{K_{NO}}{1 + K_{NO} + K_{NH_3}} \cdot P_{O_2} \tag{5}$$

Once NO is adsorbed on the peroxo complex, the rate constant for the SCR reaction is given by:

$$k_{SCR} = P_{NO} \cdot \frac{k_B T}{h} e^{\Delta S/k_B} e^{-\Delta E/k_B T} \tag{6}$$

The effect of an inhomogeneous Al-distribution is considered in the SCR reaction by different stability of the paired Cu-complexes and different equilibrium constants for K_{NO} and K_{NH3}

Considering a situation with a Cu loading of 1.6 wt %, the simulations are initialized by placing 119 $[Cu(NH_3)_2]^+$ complexes randomly in the lattice. The reaction is simulated in a temperature range from 120 to 230 °C and results are presented as averages of 10 independent simulations, which also are used to compute standard deviations. The turnover frequency (TOF) is defined as:

$$TOF = \frac{N_{NO}}{\Delta t \times N_{Cu}} \tag{7}$$

where N_{NO} is the number of NO consumed in reaction r3 within the time interval (Δt) over the number of Cu complexes, N_{Cu}. The trajectories are evolved for 10 s in real time and the simulations are performed under standard NH_3-SCR conditions at a total pressure of 1 atm, with 600 ppm NH_3, 500 ppm NO, 10 % of O_2, and balance N_2.

We perform simulations with CHA cages having different properties, denoted Type A, B and C. The stability of paired complexes has a pronounced effect on the TOF as demonstrated by comparing the results in the top and middle panels in Figure 4. The pair-stability of Type A (top panel) and Type B (middle panel) is modified by varying ΔE_1, which affects the barriers for the unpairing ($E_{r2,b}$). Type A has ΔE_1 =0.23 eV and

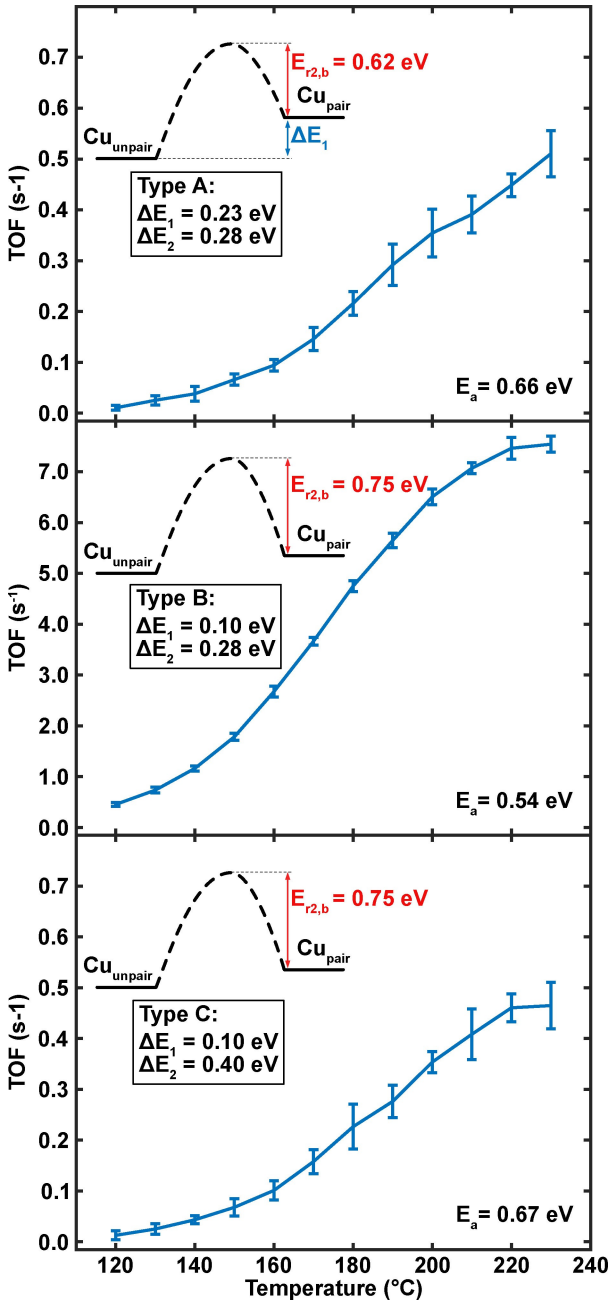

Figure 4. Simulated turnover frequency as a function of temperatures for NO conversion with standard deviations for cases with different stability of the $[Cu(NH_3)_2]^+$ pairs (ΔE_1) and the energy difference between NO and NH_3 adsorption (ΔE_2). Partial pressures: 600 ppm NH_3, 500 ppm NO and 10 % of O_2.

Type B has ΔE_1 =0.10 eV. For Type A, the reaction rate becomes appreciable at about 150 °C and reaches a value of about 0.5 s^{-1} at 230 °C. The light-off is determined by the desorption of NH_3 from $[Cu_2(NH_3)_5O_2]^{2+}$. For Type B, the TOF reaches a value of 7.5 s^{-1} at 230 °C. The difference in TOFs between Type A and Type B can to a large extent be understood by the difference in probability of having paired complexes. Using a simple Boltzmann distribution, the probability of having paired complexes increases from 0.0035 to 0.08 between Type A and Type

B, thus, a factor of about 20. The apparent activation energy is calculated to be 0.66 eV and 0.54 eV, for Type A and Type B, respectively. Thus, the apparent activation energy is reduced when the stability of the paired complex is enhanced.

Several of the Al-distributions investigated in Figure 2(e) result in an energy difference between NO and NH_3 adsorption (ΔE_2) that is higher than 0.28 eV, which is used for Type A and B. With Type C, we investigate the effect of reducing the stability of NO adsorption by using $\Delta E_2 = 0.40$ eV. The stability of NO adsorption has a marked effect on the TOF, which is reduced by a factor of 10 as compared to Type B. The apparent activation energy is in this case calculated to be 0.67 eV.

In experiments, the apparent activation energy has been measured to be in the range of 0.60 to 0.66 eV for Cu-CHA samples with a Cu-loading of about 1.6 wt % Cu.[16,41,42] Our results show that the differences in the measured apparent activation energies to some extent can be related to different Al-distributions originating from differences in synthesis procedures.

The experimental situation is most probably a CHA-material with CHA-cages having a mixture of properties. Figure 5 (top) shows the TOF for a system with both Type A and B cages, thus having two different barriers for the unpairing event. The simulations are performed for different fractions of Type A and B. The highest TOF is obtained with only Type B, and the lowest TOF is obtained with only Type A. The TOF increase with increasing amount of Type B, however, the relation is not completely linear. Taking the simulation at 200° C as an example, in the case with 50% Type A and 50% Type B, the TOF is 3.7 s^{-1}, which is slightly higher than the linear result, which corresponds to 3.4 s^{-1}. An analysis of the contribution to the TOF from the two cage types (inset) shows that Type B dominates the TOF when it is present. That Type B dominates the TOF is evident also from the apparent activation energy,

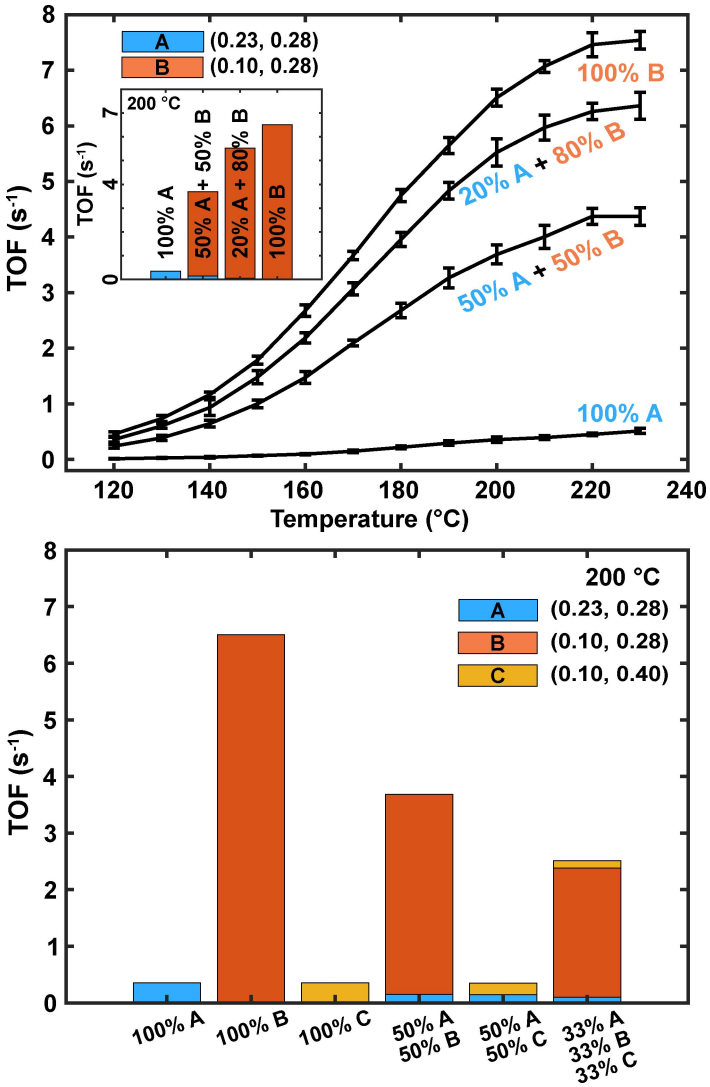

Figure 5. Top: Simulated turnover frequencies as a function of temperatures for NO conversion with standard deviations for cases with different properties of the zeolite cages. The inset shows the contribution to the TOF from the different zeolite cages at 200 °. Bottom: Simulated turnover frequencies at 200° for different properties of the zeolite cages. ΔE_1 and ΔE_2 are given in parenthesis (ΔE_1,ΔE_2). ΔE_1 is the stability of the $[Cu(NH_3)_2]^+$ pairs and ΔE_2 is the energy difference between NO and NH_3 adsorption. Partial pressures: 600 ppm NH_3, 500 ppm NO and 10% of O_2.

which is calculated to be 0.54 eV in all cases when Type B is present.

To analyze the effect of having differences in both complex-pair stability and NO/NH_3 adsorption energy, we perform simulations with Type A, B, and C cages present, Figure 5 (bottom). As already discussed, changing the stability of complex pairs keeping the adsorption energy of NO constant has a clear effect on the TOF (100% Type A compared to 100% Type B). Keeping a high stability of the complex pair, while lowering the adsorption energy of NO has also a significant effect on the TOF (100% Type B compared to 100% Type C). Combining the different types of cages shows an interesting non-linear dependencies on the TOF although Type B dominates the TOF when present. For example, in the case with 33% Type A, 33% Type B, and 33% Type C, the total TOF is 2.51 s^{-1} and the contribution from each type is 0.13, 2.28, and 0.10 s^{-1}, respectively. A completely linear relation between the TOF and the fraction of the site types would yield a total TOF of 2.41 s^{-1} and the respective contributions would be 0.12, 2.17, and 0.12 s^{-1}.

Conclusions

A density functional theory-based kinetic Monte Carlo approach has been introduced to explore the effect of the Al-distribution on the reaction kinetics of NH_3-SCR over Cu-CHA. The method is an advancement with respect to previous mean-field models as it accounts explicitly for the heterogeneity of the material given by the Al-distribution as well as the diffusion and pairing of $[Cu(NH_3)_2]^+$ complexes, which is crucial for the low-temperature activity.

The activity of the catalyst is largely determined by the stability of $[Cu(NH_3)_2]^+$ pairs and the adsorption energy of NO with respect to NH_3. Evaluating different Al-distributions with DFT calculations, shows that the stability of $[Cu(NH_3)_2]^+$ pairs can differ by as much as 0.6 eV. The difference in the NO and NH_3 adsorption energy onto the $[Cu_2(NH_3)_4O_2]^{2+}$ peroxo complex is calculated to differ also by about 0.6 eV for the different Al-distributions. The large dependence on the pair-stability and NO/NH_3 adsorption energy on the Al-distribution, yields situations where some CHA-cages are much more active for the NH_3-SCR reaction than other cages.

We find that the turn-over frequency in the kMC simulations is largely determined by the stability of the $[Cu(NH_3)_2]^+$ pairs and that the relative stability of the NO and NH_3 adsorption affects the turn-over frequency given a sufficient stability of the $[Cu(NH_3)_2]^+$ pairs. Our results reveal a hierarchy of effects influencing the performance of Cu-CHA for NH_3-SCR and link the catalytic performance with atomistic understanding.

Supporting Information

Detailed reaction cycle and elementary steps of low-temperature NH_3-SCR over Cu-CHA, and turn-over frequency as a function of the barrier for $[Cu(NH_3)_2]^+$ diffusion.

Acknowledgements

We acknowledge financial support from the Swedish Energy Agency (47110-1). The Competence Centre for Catalysis (KCK) is hosted by Chalmers University of Technology and financially supported by the Swedish Energy Agency (52689-1) and the member companies Johnson Matthey, Perstorp, Powercell, Preem, Scania CV, Umicore and Volvo Group. The calculations were performed at PDC (Stockholm) through a SNIC grant.

Conflict of Interests

The authors declare no conflict of interest.

Data Availability Statement

The data that support the findings of this study are available from the corresponding author upon reasonable request.

Keywords: Density functional theory · Cu-CHA · NH_3-SCR · kinetic Monte Carlo · Al distribution

[1] I. Nova, E. Tronconi, *Urea-SCR Technology for DeNO$_x$ After Treatment of Diesel Exhausts*; Springer Science + Business Media New York, 2014.
[2] S. J. Schmieg, S. H. Oh, C. H. Kim, D. B. Brown, J. H. Lee, C. H. Peden, D. H. Kim, *Catal. Today* **2012**, *184*, 252–261.
[3] Y. Xin, Q. Li, Z. Zhang, *ChemCatChem* **2018**, *10*, 29–41.
[4] M. Colombo, I. Nova, E. Tronconi, *Catal. Today* **2010**, *151*, 223–230.
[5] Y. Shan, X. Shi, G. He, K. Liu, Z. Yan, Y. Yu, H. He, J. Phys, *Chem. C* **2018**, *122*, 25948–25953.
[6] Y. Feng, T. V. W. Janssens, P. N. R. Vennestrøm, J. Jansson, M. Skoglundh, H. Grönbeck, J. Phys, *Chem. C* **2024**, *128*, 6689–6701.
[7] S. Shwan, M. Skoglundh, L. F. Lundegaard, R. R. Tiruvalam, T. V. W. Janssens, A. Carlsson, P. N. Vennestrøm, *ACS Catal.* **2015**, *5*, 16–19.
[8] C. Paolucci, A. A. Parekh, I. Khurana, J. R. Di Iorio, H. Li, J. D. Albarracin Caballero, A. J. Shih, T. Anggara, W. N. Delgass, J. T. Miller, *J. Am. Chem. Soc.* **2016**, *138*, 6028–6048.
[9] C. Paolucci, I. Khurana, A. A. Parekh, S. Li, A. J. Shih, H. Li, J. R. Di Iorio, J. D. Albarracin-Caballero, W. F. Schneider, R. Gounder, *Science* **2017**, *357*, 898–903.
[10] L. Chen, H. Falsig, T. V. W. Janssens, H. Grönbeck, *J. Catal.* **2018**, *358*, 179–186.
[11] C. Negri, E. Borfecchia, M. Cutini, K. A. Lomachenko, T. V. W. Janssens, G. Berlier, S. Bordiga, *ChemCatChem* **2019**, *11*, 3828–3838.
[12] C. Paolucci, J. R. Di Iorio, W. F. Schneider, R. Gounder, *Acc. Chem. Res.* **2020**, *53*, 1881–1892.
[13] F. Gao, D. Mei, Y. Wang, J. Szanyi, C. H. Peden, *J. Am. Chem. Soc.* **2017**, *139*, 4935–4942.
[14] X. Wang, L. Chen, P. N. R. Vennestrøm, T. V. W. Janssens, J. Jansson, H. Grönbeck, M. Skoglundh, *ChemCatChem* **2021**, *13*, 2577–2582.
[15] L. Chen, T. V. W. Janssens, P. N. R. Vennestrøm, J. Jansson, M. Skoglundh, H. A. Gr"onbeck, *ACS Catal.* **2020**, *10*, 5646–5656.
[16] Y. Feng, X. Wang, T. V. W. Janssens, P. N. R. Vennestrøm, J. Jansson, M. Skoglundh, H. Grönbeck, *ACS Catal.* **2021**, *11*, 14395–14407.
[17] Y. Feng, T. V. W. Janssens, P. N. R. Vennestrøm, J. Jansson, M. Skoglundh, H. Grönbeck, *J. Phys. Chem. C* **2021**, *125*, 4595–4601.
[18] Y. Feng, D. Creaser, H. Grönbeck, *Top. Catal.* **2022**, *2* .
[19] L. Chen, H. Falsig, T. V. W. Janssens, J. Jansson, M. Skoglundh, H. Grönbeck, *Catal. Sci. Technol.* **2018**, *8*, 2131–2136.
[20] D. T. Gillespie, *J. Comput. Phys.* **1976**, *22*, 403–434.
[21] K. A. Fichthorn, W. H. Weinberg, *J. Chem. Phys.* **1991**, *95*, 1090–1096.
[22] M. Salciccioli, M. Stamatakis, S. Caratzoulas, D. G. Vlachos, *Chem. Eng. Sci.* **2011**, *66*, 4319–4355.

[23] M. Jørgensen, L. Chen, H. Grönbeck, J. Phys, *Chem. C* **2018**, *122*, 20351–20357.
[24] A. Bruix, J. T. Margraf, M. Andersen, K. Reuter, *Nature Catalysis* **2019**, *2*, 659–670.
[25] G. Kresse, J. Hafner, *Phys. Rev. B: Condens. Matter Mater. Phys.* **1993**, *48*, 13115–13118.
[26] G. Kresse, J. Hafner, *Phys. Rev. B: Condens. Matter Mater. Phys.* **1994**, *49*, 14251–14269.
[27] G. Kresse, J. Furthmüller, *Phys. Rev. B: Condens. Matter Mater. Phys.* **1996**, *54*, 11169–11186.
[28] G. Kresse, J. Furthüller, *Comput. Mater. Sci.* **1996**, *6*, 15–50.
[29] P. E. Blöchl, *Phys. Rev. B: Condens. Matter Mater. Phys.* **1994**, *50*, 17953–17979.
[30] G. Kresse, D. Joubert, *Phys. Rev. B: Condens. Matter Mater. Phys.* **1999**, *59*, 1758–1775.
[31] J. P. Perdew, K. Burke, M. Ernzerhof, *Phys. Rev. Lett.* **1996**, *77*, 3865–3868.
[32] L. Y. Isseroff, E. A. Carter, *Phys. Rev. B: Condens. Matter Mater. Phys.* **2012**, *85*, 1–7.
[33] L. Chen, T. V. W. Janssens, H. Gr"onbeck, *Phys. Chem. Chem. Phys.* **2019**, *21*, 10923–10930.
[34] S. Grimme, J. Antony, S. Ehrlich, H. Krieg, *J. Chem. Phys.* **2010**, *132*, 154104.
[35] S. Grimme, S. Ehrlich, L. Goerigk, *J. Comput. Chem.* **2012**, *32*, 1456–1465.
[36] F. Gao, E. D. Walter, M. Kollar, Y. Wang, J. Szanyi, C. H. Peden, *J. Catal.* **2014**, *319*, 1–14.
[37] F. Gao, N. Washton, Y. Wang, M. Koll'ar, J. Szanyi, C. Peden, *J. Catal.* **2015**, *331*, 25–38.
[38] I. Chorkendorff, J. W. Niemantsverdriet, *Concepts of Modern Catalysis and Kinetics*, John Wiley & Sons, **2017**, p 109.
[39] L. Chen, J. Jansson, M. Skoglundh, H. Grönbeck, *J. Phys. Chem. C* **2016**, *120*, 29182–29189.
[40] A. P. J. Jansen, *An Introduction to Kinetic Monte Carlo Simulations of Surface Reactions*., electronic ed.; Springer Berlin Heidelberg, 2012; pp 22, 53, and 162.
[41] S. A. Bates, A. A. Verma, C. Paolucci, A. A. Parekh, T. Anggara, A. Yezerets, W. F. Schneider, J. T. Miller, W. N. Delgass, F. H. Ribeiro, *J. Catal.* **2014**, *312*, 87–97.
[42] A. J. Shih, Synthesis and Characterization of Copper-Exchanged Zeolite Catalysts and Kinetic Studies on No_x Selective Catalytic Reduction With Ammonia. Ph.D. thesis, 2018.

Manuscript received: May 15, 2024
Revised manuscript received: June 27, 2024
Accepted manuscript online: June 28, 2024
Version of record online: August 26, 2024